IEEE Photonics Journal
An IEEE Photonics Society Publication

Open Access

Numerical Investigation of Phase-Conjugate Wave Generation as a Pulse Cleaner in Femtosecond Petawatt Laser Systems

Volume 11, Number 3, June 2019

Ziruo Cui
Xinglong Xie
Jun Kang
Qingwei Yang
Meizhi Sun
Ailin Guo
Haidong Zhu
Ping Zhu
Qi Gao
Xiao Liang
Simin Zhang
Jianqiang Zhu

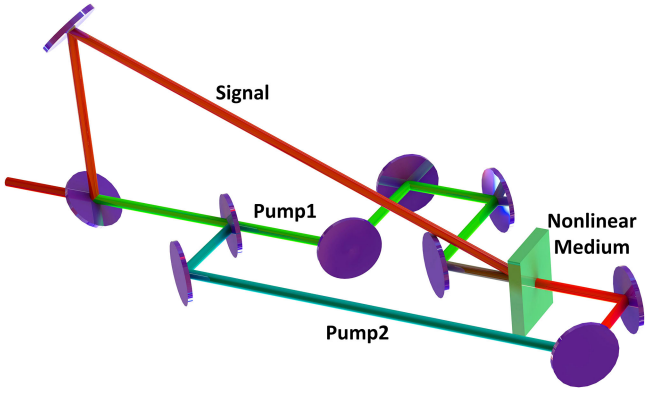

DOI: 10.1109/JPHOT.2019.2911099
1943-0655

IEEE photonics SOCIETY

IEEE

Numerical Investigation of Phase-Conjugate Wave Generation as a Pulse Cleaner in Femtosecond Petawatt Laser Systems

Ziruo Cui,[1,2] **Xinglong Xie**,[1] **Jun Kang**,[1] **Qingwei Yang**,[1] **Meizhi Sun**,[1] **Ailin Guo**,[1] **Haidong Zhu**,[1] **Ping Zhu**,[1] **Qi Gao**,[1] **Xiao Liang**,[1] **Simin Zhang**,[1] **and Jianqiang Zhu**[1]

[1]Key Laboratory of High Power Laser and Physics, Shanghai Institute of Optics and Fine Mechanics, Chinese Academy of Sciences, Shanghai 201800, China
[2]University of Chinese Academy of Sciences, Beijing 100049, China

DOI:10.1109/JPHOT.2019.2911099

Manuscript received January 4, 2019; revised March 31, 2019; accepted April 9, 2019. Date of publication April 17, 2019; date of current version May 7, 2019. This work was supported in part by the National Natural Science Foundation of China under Grants 11304332, 11704392, and 61705245, and in part by the International Partnership Program of Chinese Academy Of Sciences under Grant 181231KYSB20170022. Corresponding author: Ziruo Cui (email: ziruocui@siom.ac.cn).

Abstract: We report on comprehensive research regarding the potential of phase-conjugate wave (PCW) generation via backward degenerate four-wave mixing process as a pulse cleaner in femtosecond high-power laser systems. We analyzed the performance of this technique by investigating the contrast enhancement capability, gain bandwidth, and energy conversion efficiency. All of these parameters are important in pulse cleaning. The numerical calculations verified that a considerably large efficiency bandwidth product and an excellent contrast enhancement capability can be realized by finding a balance between each physical effect. The simulation results based on this study provide guidance for the application of this technique in laser systems with different bandwidths. The method, which is based on PCW generation, provides new insights for femtosecond petawatt laser systems as pulse cleaners.

Index Terms: Phase-conjugate wave generation, degenerate four-wave mixing process, contrast enhancement, petawatt laser systems.

1. Introduction

Owing to the remarkable progress in the chirped pulse amplification (CPA) and optical parametric chirped pulse amplification (OPCPA) techniques, several petawatt-class laser facilities have been built, achieving a high output laser intensity in the range of 10^{21}–10^{22} W/cm^2 [1]–[5]. Such an intense laser provides a powerful tool for the experimental study of laser–matter interactions in the relativistic regime [6]–[9]. A crucial parameter of ultrashort high peak power laser systems in high field experiments is the temporal contrast ratio, which is defined as the intensity ratio of the main pulse to the background noise. A poor contrast ratio indicates strong pre-pulses or a pedestal before the main pulse. Intense pre-pulses or background noise can modify or even

destroy the target structure, generate pre-plasma, and as a result, change the interaction mechanism [10], [11]. For a petawatt laser system, a typical temporal contrast ratio in the range of 10^{11}–10^{12} is required. Unfortunately, without the application of any pulse cleaning technique, the temporal contrast of the focal spot is several orders of magnitude lower than the required level.

A number of techniques have been proposed and investigated experimentally over the past 20 years aiming to improve the temporal contrast of high peak power laser systems. These methods include the application of saturable absorbers [12], a nonlinear Sagnac interferometer [13], a double CPA scheme [14], nonlinear birefringence [15], cross-polarization wave generation (XPW) [16], a low-gain optical parametric amplification (OPA) [17], self-diffraction (SD) process [18], second-harmonic generation [19], spatial chirp technique [20], methods based on nonlinear Fourier-filter [21], rapid scanning Fabry–Perot (F–P) interferometer [22], plasma mirrors [23], and picosecond-pumped OPCPA (PS-OPCPA) [24]. Among these, XPW, plasma mirrors, and PS-OPCPA are the most promising techniques, which have already been applied combined or independently in several petawatt-class laser facilities around the world [25]–[30]. However, these techniques are still theoretically or technically limited, especially in engineering applications, which requires the development of novel methods in contrast improvement.

In 2012, Liang *et al*. proposed a novel contrast enhancement method based on phase-conjugate wave (PCW) generation via a degenerate four-wave mixing (DFWM) process [31]. A proof of principle experiment was conducted using a picosecond unchirped pulse with a bandwidth of several nanometers and energy at level of several hundred microjoules. The PCW was generated via the backward DFWM process with an energy conversion efficiency of 10% and a contrast ratio five orders higher than that of the input pulse. Compared with XPW, this method has better contrast enhancement capability owing to the lack of polarizers which limits the performance of the XPW method. The results in Ref. [31] proved that the method based on PCW generation is a suitable technique for pulse cleaning in picosecond ultra-intense laser systems. However, there has been few research on the performance of this method applicable to femtosecond laser systems with a spectral bandwidth of 50 nm or broader. This needs to be studied systematically, as the DFWM process strongly affects the gain bandwidth of the spectrum in a broad bandwidth laser system. As a result, the temporal profile is possibly affected when the PCW is finally compressed to the femtosecond range. Moreover, the contrast of the PCW following compression presents a more complicated pattern compared with that of the PCW without compression, which needs to be carefully studied.

In this paper, we present a comprehensive study on the potential of PCW generation in femtosecond laser systems, based on the backward DFWM process as a pulse cleaner. The simulations focused on the contrast enhancement capability, the gain bandwidth of the spectrum, and the energy conversion efficiency, as these are all key parameters to evaluate the performance of pulse cleaners in broad-bandwidth laser systems. Specifically, a recursive formula is established to determine the contrast ratio of the PCW directly after the DFWM process, which can numerically study the contrast evolution in other nonlinear processes, such as XPW, sum-frequency generation, and frequency doubling. A pedestal noise within a duration of few picoseconds or broader was found when the contrast of the PCW after pulse compression was analyzed. The origin and the method of the removal of this pedestal noise were studied. Next, we examined the optimization of the gain bandwidth of the PCW to realize a minimally compressible pulse width. The systematic requirement of the input pulse width for the DFWM process was determined for laser systems with different bandwidths. Additionally, the simulation results proved that the conversion efficiency is mainly affected by the spatial–temporal profile and the pump–signal intensity ratio of the input fields. The numerical calculations verified that a considerably high efficiency bandwidth product and excellent contrast enhancement capacity could be realized by finding a balance between each physical effect and input parameters. The simulation results in this study provide guidance for applying this technique in laser systems with a wide range of bandwidth.

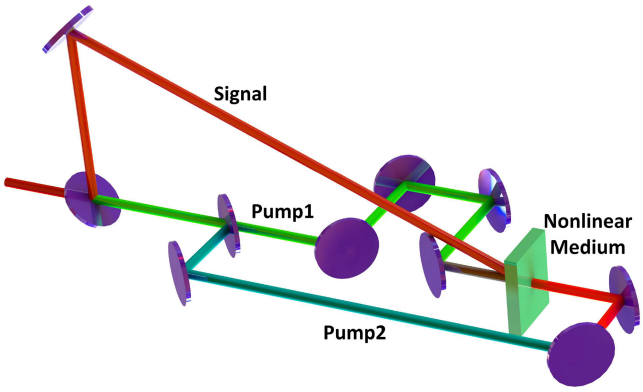

Fig. 1. Schematic image of the PCW generation by backward DFWM process.

2. Numerical Modelling

The PCW can be generated through many physical processes such as degenerate four-wave mixing process in Kerr medium [32], stimulated Brillouin scattering [33], backward stimulated emission [34] and photo-refractive effects [35], [36]. Among these physical processes, the DFWM process is a promising mechanism to generate PCW with high efficiency. The physical mechanism of the DFWM process in Kerr medium is an instantaneous third-order nonlinear process arises from the distortion of electron cloud. According to the principle of the backward DFWM, two photons from the pumps are annihilated and two photons are added to each of the signal and the PCW. When the phase-matching condition is satisfied, the PCW is generated and the signal is amplified.

A schematic image of the backward DFWM process based on third-order nonlinear response is shown in Fig. 1, where the different input fields are denoted by “Pump1”, “Pump2” and “Signal”, respectively. In an experimental arrangement, one laser beam is separated into three beams, with two pump beams with high energy counter-propagating and hitting the opposite surfaces of the nonlinear medium, and the wave vector of the third beam (Signal) with weak energy is slightly misaligned with a small angle with respect to Pump1. The angle must be small to achieve a long interaction length. The phase-matching condition is automatically satisfied in an isotropic medium for degenerate inputs, i.e., $\omega_1 = \omega_2 = \omega_3 = \omega_4$ when the two counter-propagating pumps have equal intensity. This can be explained by the conservation of energy and momentum of the photons in the DFWM process. Thus, whenever Pump1, Pump2, and Signal are perfectly synchronized in the time domain and coupled properly in the space domain, a PCW can be generated and amplified in the opposite direction of the signal. It should be noted that if the two input pumps have different energy or are not perfectly counter-propagating, the phase-matching condition breaks and the conversion efficiency of the PCW would reduce significantly. In order to achieve a high energy conversion efficiency of the PCW, a centrally symmetric medium needs to be chosen so that second-order nonlinear effects are negligible.

The coupled wave equations describing the DFWM process based on third-order nonlinear response in a lossless nonlinear medium in terms of diffraction, dispersion and nonlinear effects are given by:

$$\frac{\partial A_1}{\partial z} = \cos\theta_1 \left[\frac{1}{2k_1}\nabla_\perp^2 - i\tan\rho_1 \frac{\partial}{\partial x}\right] A_1 + \cos\theta_1 \left[i\frac{\beta_2}{2}\frac{\partial^2}{\partial \tau^2} - \frac{\beta_3}{6}\frac{\partial^3}{\partial \tau^3} + \cdots\right] A_1$$
$$+ \cos\theta_1 \frac{3i\omega_1}{2n_1 c}\chi^{(3)}(\omega_1) \cdot \left[\left(|A_1|^2 + 2|A_2|^2 + 2|A_3|^2 + 2|A_4|^2\right) A_1 + 2A_2^* A_3 A_4 e^{\Delta kz}\right]$$

$$\begin{aligned}
\frac{\partial A_2}{\partial z} &= \cos\theta_2\left[\frac{1}{2k_2}\nabla_\perp^2 - i\tan\rho_2\frac{\partial}{\partial x}\right]A_2 + \cos\theta_2\left[i\frac{\beta_2}{2}\frac{\partial^2}{\partial\tau^2} - \frac{\beta_3}{6}\frac{\partial^3}{\partial\tau^3} + \cdots\right]A_2 \\
&\quad + \cos\theta_2\frac{3i\omega_2}{2n_2c}\chi^{(3)}(\omega_2)\cdot\left[\left(|A_2|^2 + 2|A_1|^2 + 2|A_3|^2 + 2|A_4|^2\right)A_2 + 2A_1^*A_3A_4e^{\Delta kz}\right] \\
\frac{\partial A_3}{\partial z} &= \cos\theta_3\left[\frac{1}{2k_3}\nabla_\perp^2 - i\tan\rho_3\frac{\partial}{\partial x}\right]A_3 + \cos\theta_3\left[i\frac{\beta_2}{2}\frac{\partial^2}{\partial\tau^2} - \frac{\beta_3}{6}\frac{\partial^3}{\partial\tau^3} + \cdots\right]A_3 \\
&\quad + \cos\theta_3\frac{3i\omega_3}{2n_3c}\chi^{(3)}(\omega_3)\cdot\left[\left(|A_3|^2 + 2|A_1|^2 + 2|A_2|^2 + 2|A_4|^2\right)A_3 + 2A_4^*A_1A_2e^{-\Delta kz}\right] \\
\frac{\partial A_4}{\partial z} &= \cos\theta_4\left[\frac{1}{2k_4}\nabla_\perp^2 - i\tan\rho_4\frac{\partial}{\partial x}\right]A_4 + \cos\theta_4\left[i\frac{\beta_2}{2}\frac{\partial^2}{\partial\tau^2} - \frac{\beta_3}{6}\frac{\partial^3}{\partial\tau^3} + \cdots\right]A_4 \\
&\quad + \cos\theta_4\frac{3i\omega_4}{2n_4c}\chi^{(3)}(\omega_4)\cdot\left[\left(|A_4|^2 + 2|A_1|^2 + 2|A_2|^2 + 2|A_3|^2\right)A_4 + 2A_3^*A_1A_2e^{-\Delta kz}\right] \qquad (1)
\end{aligned}$$

Here, $A_{m,m=1\ldots4}$ represent the complex amplitudes of the two pumps, the signal, and the PCW, respectively, and $A^*_{m,m=1\ldots4}$ are their complex conjugates. In an isotropic medium, the phase mismatching parameter Δk is always zero in the case of degenerate inputs. The first terms in the right-hand side represent the spatial effects (diffraction and walk-off) while the second terms are associated with the dispersion (group velocity dispersion (GVD) and high-order dispersion) of the nonlinear medium. The third terms describe the effects of self-phase modulation (SPM), cross-phase modulation (XPM), and the parametric amplification (PA).

Equation (1) can be modeled numerically by using a split-step iteration approach, which divides a nonlinear medium into N slices. For each slice, Eq. (1) is broken into different equations, which can be solved independently. Generally, when the angles between the input pumps and the signal are small with respect to the z-axis, i.e., $\cos\theta_1 = \cos\theta_2 \approx 1, \cos\theta_3 = \cos\theta_4 \approx 1$, for the degenerate case, Eq. (1) can be rewritten as follows:

$$\frac{\partial\vec{W}}{\partial z} = \left(\hat{S} + \hat{T} + \hat{N}\right)\cdot\vec{W}, \qquad (2)$$

Here $\hat{S}$, $\hat{T}$ and $\hat{N}$ represent spatial, temporal, and nonlinear operators, respectively. The symbolic solution is given by:

$$\vec{W}(z+dz) \approx \vec{W}(z)\cdot e^{\hat{S}dz}e^{\hat{T}dz}e^{\hat{N}dz}. \qquad (3)$$

The spatial and temporal effects can be considered in the frequency domain by adding the corresponding phase terms in Eq. (3). Similarly, the nonlinear step describes the third-order nonlinear effects in the DFWM process, including SPM, XPM, and PA. This step is numerically calculated using a fourth-order Runge–Kutta algorithm.

3. Simulation Results

In this section, the numerical investigation of the contrast enhancement capability, gain bandwidth, and the energy conversion efficiency of the PCW by the DFWM process is presented. To model the DFWM process numerically, we built a three-dimensional data matrix comprising an array of $R_{64\times64\times16384}(x, y, t) \times L_{128}(z)$ for describing each wave (pumps, signal and PCW). The input fields can be defined as follows:

$$E_i = A_i(x, y)\cdot e^{-\left(4\ln 2\cdot\frac{t^2}{\tau_i^2}\right)}\cdot e^{j(1+c_it)}\cdot e^{j\omega_0 t},\ i = 1:4 \qquad (4)$$

where τ_i represent the full width at half maximum (FWHM) pulse widths of each wave, and c_i describe the corresponding initial temporal chirp ratios.

3.1. Contrast Enhancement Capability

The contrast enhancement capability of the DFWM process as a pulse cleaner in femtosecond laser systems was investigated by the simulation of the contrast ratio of the PCW generated in the DFWM process. In a femtosecond broad bandwidth laser system, the amplified PCW generated via the DFWM process must be compressed to a minimal pulse width to realize maximal output intensity. Consequently, the information on the contrast ratio of the PCW following pulse compression is even more important than that without compression. In this section, a recursive formula is established to investigate the contrast evolution of the PCW in the DFWM process. The contrast of the PCW after pulse compression was theoretically studied; a convenient standard to optimize the contrast of the PCW after compression for laser systems with different bandwidths was provided.

3.1.1 Contrast Ratio Without Pulse Compression: The contrast of the PCW without compression is determined. The contrast of each field in the DFWM process can be studied by the simulation of the amplitude of each field. For the simulation, a recursive formula was established to numerically calculate the contrast of each field as a function of the interaction length. The recursive formula is given by

$$C_i(Z+\Delta z)=\left[\frac{\left|A_i(Z)\sqrt{C_i(Z)}+\Delta A_i(Z,Z+\Delta z)\sqrt{C'_i(Z)}\right|}{|A_i(Z)+\Delta A_i(Z,Z+\Delta z)|}\right]^2, i=1\cdots 4. \tag{5}$$

where $A_{i,i=1\cdots4}(Z)$ are the complex amplitudes of electric fields at a given position Z; the increments of the amplitude from position Z to $Z+\Delta z$ are represented by $\Delta A_i(Z,Z+\Delta z)$, and the contrast ratio of $A_i(Z)$ and $\Delta A_i(Z,Z+\Delta z)$ are represented by $C_i(Z)$ and $C'_i(Z)$, respectively. The general formula for the contrast of each field can be obtained by rearranging Eq. (5) as:

$$\begin{aligned}
|A_i(N+1)|^2\cdot C_i(N+1)&=|A_i(N)|^2\cdot C_i(N)\\
&\quad+|\Delta A_i(N)|^2\cdot C'_i(N)\\
&\quad\mp|A_i(N)\cdot\Delta A_i(N)|\sqrt{C_i(N)\cdot C'_i(N)},\\
N\geq 3, i&=1\cdots4\\
|A_i(N)|^2\cdot C_i(N)&=|A_i(N-1)|^2\cdot C_i(N-1)\\
&\quad+|\Delta A_i(N-1)|^2\cdot C'_i(N-1)\\
&\quad\mp|A_i(N-1)\cdot\Delta A_i(N-1)|\sqrt{C_i(N-1)\cdot C'_i(N-1)},\\
&\quad\vdots\\
|A_i(2)|^2\cdot C_i(2)&=|A_i(1)|^2\cdot C_i(1)\\
&\quad+|\Delta A_i(1)|^2\cdot C'_i(1)\\
&\quad\mp|A_i(1)\cdot\Delta A_i(1)|\sqrt{C_i(1)\cdot C'_i(1)}.
\end{aligned}\tag{6}$$

By summing each line of Eq. (6), the general formula for contrast evolution can be obtained:

$$\begin{aligned}
C_i(N+1)&=\frac{1}{|A_i(N+1)|^2}\\
\cdot\left|A_i(1)^2\cdot C_i(1)+\sum_{j=1}^{N}\Delta A_i(j)^2\cdot C'_i(j)+2\sum_{j=1}^{N}A_i(j)\cdot\Delta A_i(j)\cdot\sqrt{C_i(j)\cdot C'_i(j)}\right|,\\
N\geq 2, i&=1\cdots4.
\end{aligned}\tag{7}$$

Similarly, an inverse relation can be obtained for the pumps from the energy conservation. Eq. (7) provides a straightforward method to estimate the evolution of contrast ratio. As the amplitude increment ΔA_i and the corresponding contrast C'_i can be calculated numerically, the contrast ratio

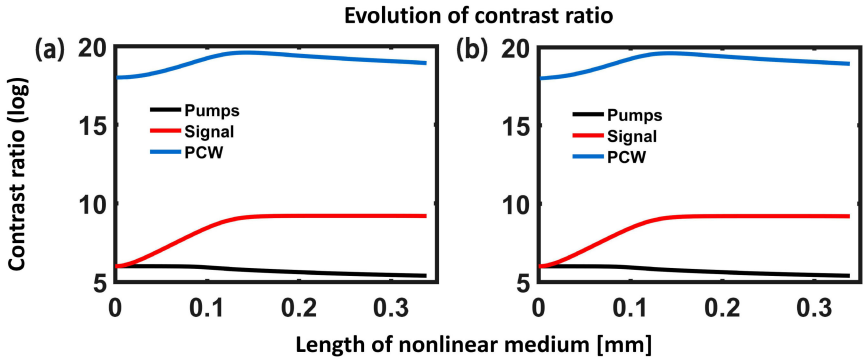

Fig. 2. Contrast evolution of each field (In case $\kappa = 40$): (a) direct calculation the contrast by a simulation the envelop evolution of each field and (b) calculated by Eq. (7).

$C_i(N+1)$ can also be determined when the amplitude $A_i(1)$ and contrast $C_i(1)$ of the input field are selected. Thus, the contrast evolution of each field can be determined by this method.

A quantitative simulation result of the contrast evolution in the DFWM process is shown in Fig. 2, where the input fields are assumed to have the same contrast ratio of 10^6. We define parameter $\kappa = A_1(1)/A_3(1)$ to represent the pump–signal ratio of input amplitude, and in this case $\kappa = 40$. The contrast ratio shown in Fig. 2(a) is obtained by direct calculation based on the simulation of the evolution of the complex amplitudes, while Fig. 2(b) presents the numerical calculation using Eq. (7). A good agreement is achieved in Figs. 2(a) and 2(b), which verifies the validity of Eq. (7). As shown in Fig. 2, the contrast ratio of each field exhibited different evolution patterns as the length of the nonlinear medium increased. Further, the pump contrast deteriorates slightly from 10^6 to $10^{5.4}$ during the parametric process while opposite trends can be seen in both the signal and the PCW (improvement from 10^6 to $10^{9.2}$ and from 10^{18} to $10^{19.6}$, respectively). Additionally, the contrast of each field shows a saturating tendency together with the energy conversion. Consequently, the optimal condition for contrast enhancement is achieved when the energy conversion of the PCW is optimized.

It should be noted that Eq. (7) is not only suitable for the simulation of the contrast evolution of the DFWM process but also convenient for the numerical study of the contrast evolution in other nonlinear processes, such as XPW, sum-frequency generation, and frequency-doubling.

3.1.2 Contrast Ratio Following Compression: Unlike picosecond narrow bandwidth laser systems, the amplified signal in a femtosecond broad bandwidth laser system needs to be compressed to a minimal pulse width to realize maximal output intensity. A comparison of the contrast ratio between the PCW and signal without performing the DFWM process is shown in Fig. 3, where the input fields have a pulse width of 1 ps and a bandwidth (FWHM) of 50 nm. The contrast of the PCW directly after the DFWM process (without compression) and that of the signal without performing the DFWM process are shown in Fig. 3(a), while the compressed counterparts are shown in Fig. 3(b).

As shown in Fig. 3(a), the patterns of contrast of the PCW and signal without compression are similar, while there is a significant difference between the PCW and signal following compression, as shown in Fig 3(b). The contrast of the compressed PCW consists of three temporal regions: a rapid growing region, in which the contrast of the PCW increases from 10^6 to 10^{15} ($>$8 ps region), a pedestal region, where the contrast of the PCW remained stable and nearly equivalent to that of the signal (this region ranges from approximately $\pm$0.6–8 ps), and the main pulse region. A straightforward conclusion can be drawn that the contrast of the compressed PCW increased dramatically compared with that of the signal in the temporal region (from 8 ps to a few ns in logarithmic coordinates) before the main pulse, which verified that the DFWM process is capable of generating a PCW pulse with better contrast ratio compared with the signal, regardless of compression. A potential drawback that limits the application of the DFWM process as a pulse cleaner in a femtosecond laser system, is that although the contrast of the compressed PCW can

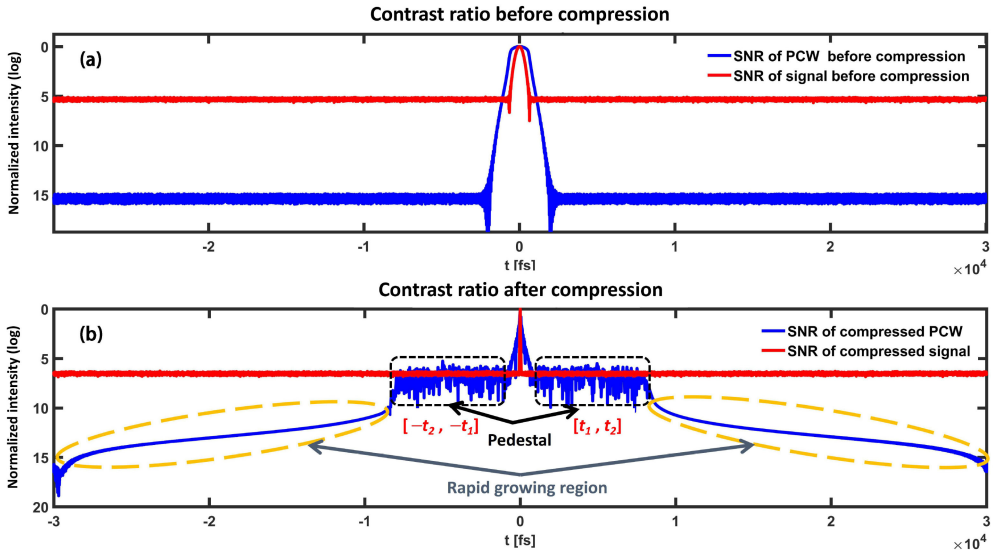

Fig. 3. Contrast ratios of the PCW and signal before and after compression: (a) contrast ratio of the PCW and signal before compression and (b) contrast ratio of the PCW and signal after compression. The red lines represent the contrast ratios of the signal and the blue lines represent the contrast ratios of the PCW.

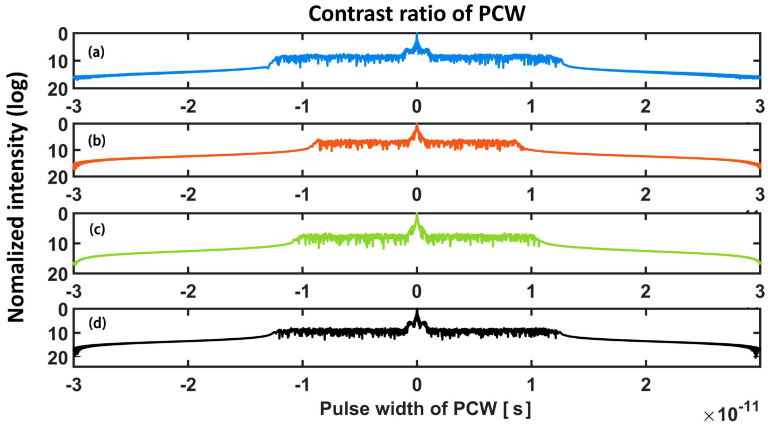

Fig. 4. The contrast ratio of the PCW after compression by considering the effects of PA, SPM, and XPM: (a) contrast ratio of the PCW considering the effects of the PA, SPM and XPM, (b) contrast ratio of the PCW considering the effects of the PA and SPM, and (c) contrast ratio of the PCW considering the effects of the PA and XPM, (d) contrast ratio of the PCW only considering the effect of PA.

be improved dramatically in the region approximately 10 ps before the main pulse, the contrast within a few ps (the pedestal region) is comparable with that of the input fields.

In order to improve the contrast ratio of the PCW within the pedestal region, the physical origin of the pedestal noise was numerically investigated. This procedure was performed by the analysis of the effect of each term associated with the nonlinear effects in Eq. (1). The contrast of the compressed PCW without considering phase modulation (PM) effects is shown in Fig. 4.

As shown in Fig. 4, the pedestal noise of the PCW exists as long as the effect of the PA is considered, which indicates that the pedestal noise arises from the PA process. As shown in Figs. 4(b)–(d), the duration of the pedestal noise is affected by the SPM and XPM by spectral modulation. Strong spectral modulation results in an enormous modulation in the spectrum intensity

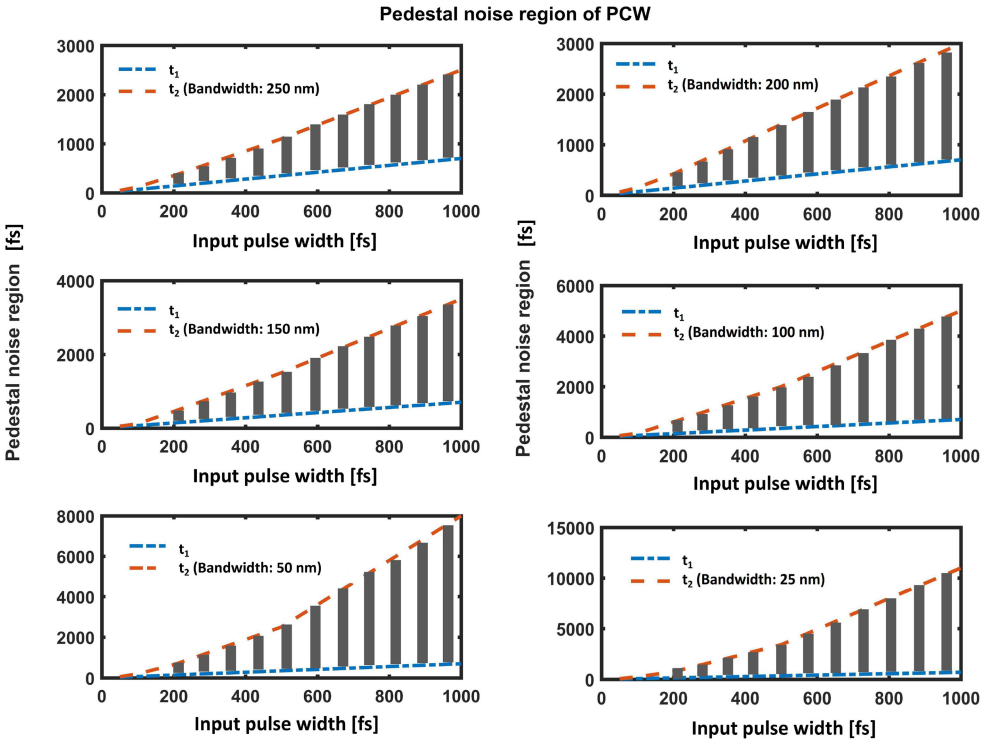

Fig. 5. Relationship between the pedestal noise duration [t_1, t_2] and the input pulse width for laser systems with different bandwidths.

and phase, and finally creates pre-pulses when the PCW is compressed, even if these pre-pulses are undetectable before compression.

Further analysis shows that the duration of the pedestal noise is fundamentally determined by the pulse width (chirp ratio) and initial bandwidth of the input fields. The relationship between the pedestal duration and the pulse width of the input fields for laser systems with different bandwidths is numerically calculated and shown in Fig. 5, where the pedestal noise is defined in the range of [$-t_2$, $-t_1$] and [t_1, t_2] around the main pulse. As shown in Fig. 5, the duration of the pedestal region is strongly affected by the pulse width of input fields: the start time $t_1 \approx 0.7t_0$ (t_0 represents the pulse width of input fields) while the termination time t_2 grows sharply as the input pulse width increases. Additionally, the pedestal duration is approximately inversely proportional to the bandwidth of input fields because the termination time t_2 varies sharply with input bandwidth. With the broadening of the input bandwidth, the pedestal region becomes narrower. Fig. 5 also indicates that the duration of the pedestal noise is roughly proportional to the chirp ratio of input fields. For laser systems with given bandwidths, a relatively narrow pulse width (small chirp ratio) of input fields can surely result in a reduction of the pedestal duration. As a result, Figure 5 provides a convenient standard to restrict the pedestal interval for laser systems with different bandwidths.

3.2. Gain Bandwidth

An ideal pulse cleaner in a broad bandwidth laser system is capable of enhancing the pulse contrast without reducing the bandwidth of the input fields which determines the minimal compressible pulse width to realize maximal output power. In this section, the initial chirp and nonlinear effects were investigated, and the working conditions for the DFWM process are optimized in femtosecond laser systems with different bandwidths. Simulation results indicate that the optimized PCW is capable to be compressed to narrower than input fields regardless of the bandwidth of input fields.

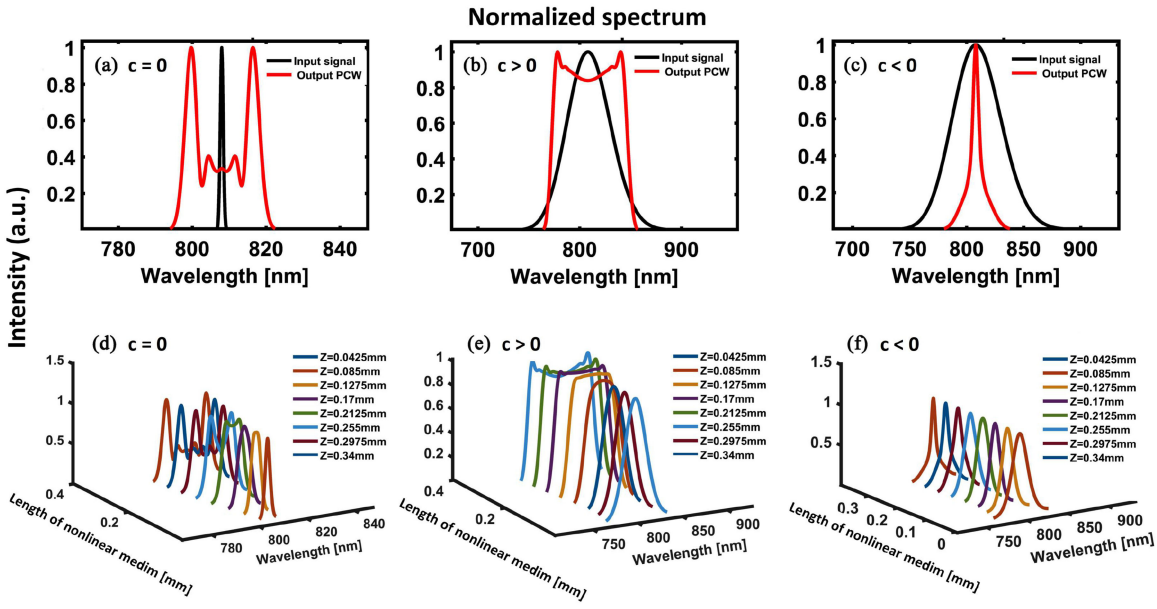

Fig. 6. Gain bandwidths of the PCW. (a)–(c) gain bandwidth of PCW compared with the input signal: (a) non-chirped inputs, (b) positive chirped signal resulting in a broadening of the PCW gain bandwidth, and (c) negative chirp signal resulting in the narrowing of the bandwidth. (d)–(f) evolution of gain bandwidth of the PCW: (d) non-chirped inputs, (e) initially positive chirp, and (f) initially negative chirp.

3.2.1 Effect of the Initial Chirp: The bandwidth of the amplified PCW was simulated for non-chirped, positive-chirped, and negative-chirped inputs. As shown in Fig. 6, the bandwidth of each field grows broader in the DFWM process as a result of effects (SPM and XPM) for inputs that are initially non-chirped. For initially positive-chirped inputs, the PM effects introduced bandwidth growth is counterbalanced by PM induced gain narrowing, resulting in a sharper spectrum profile regardless of the broadening of the spectrum. The initially negative-chirped inputs, by contrast, give a different result because the SPM and XPM induced frequency-chirps have a negative sign compared with the initial chirp, resulting in a significantly narrower gain bandwidth of the output fields than those of the inputs. Thus, an initially positive-chirped or nearly non-chirped signal should be utilized as input fields in the DFWM process.

3.2.2 Optimization of the Minimal Compressible Pulse Width of the PCW: The minimal compressible pulse width of the PCW was optimized for input fields with initial positive-chirp ratio in the DFWM process. As the initial chirp ratio has a strong effect on the bandwidth of the PCW, for laser systems with different bandwidths, an appropriate choice of initial chirp ratio in the DFWM process has crucial importance in the broadening of the gain bandwidth of the PCW and, as a result, in the optimization of the minimal compressible pulse width. To satisfy this requirement, we gradually scaled the initial bandwidth from 5 to 200 nm and simulated the temporal profile of the compressed PCW with different input pulse widths (i.e., chirp ratio). The minimal compressible pulse width was calculated by depriving the linear-chirp, meaning the introduction of corresponding negative linear-chirp to the complex amplitudes of the PCW and the input fields. The compressed temporal profiles of the PCW with different input pulse widths are shown in Fig. 7 where the initial bandwidths are chosen as 5, 25, 50, 100, 150 and 200 nm. The straightforward conclusion that can be drawn from Fig. 8 is that the minimal compressible pulse width of the PCW decreases monotonically when the input pulse width is narrowed, regardless of the value of the initial bandwidth. Furthermore, the compressed pulse width of the PCW decreases from 60 to 13 fs when the initial bandwidth was 5 nm (Fig. 7(a)). Similar trends are presented in Figs. 7(b)–7(f); the pulse width of the PCW with different input bandwidths can be compressed to the corresponding optimized values as the input

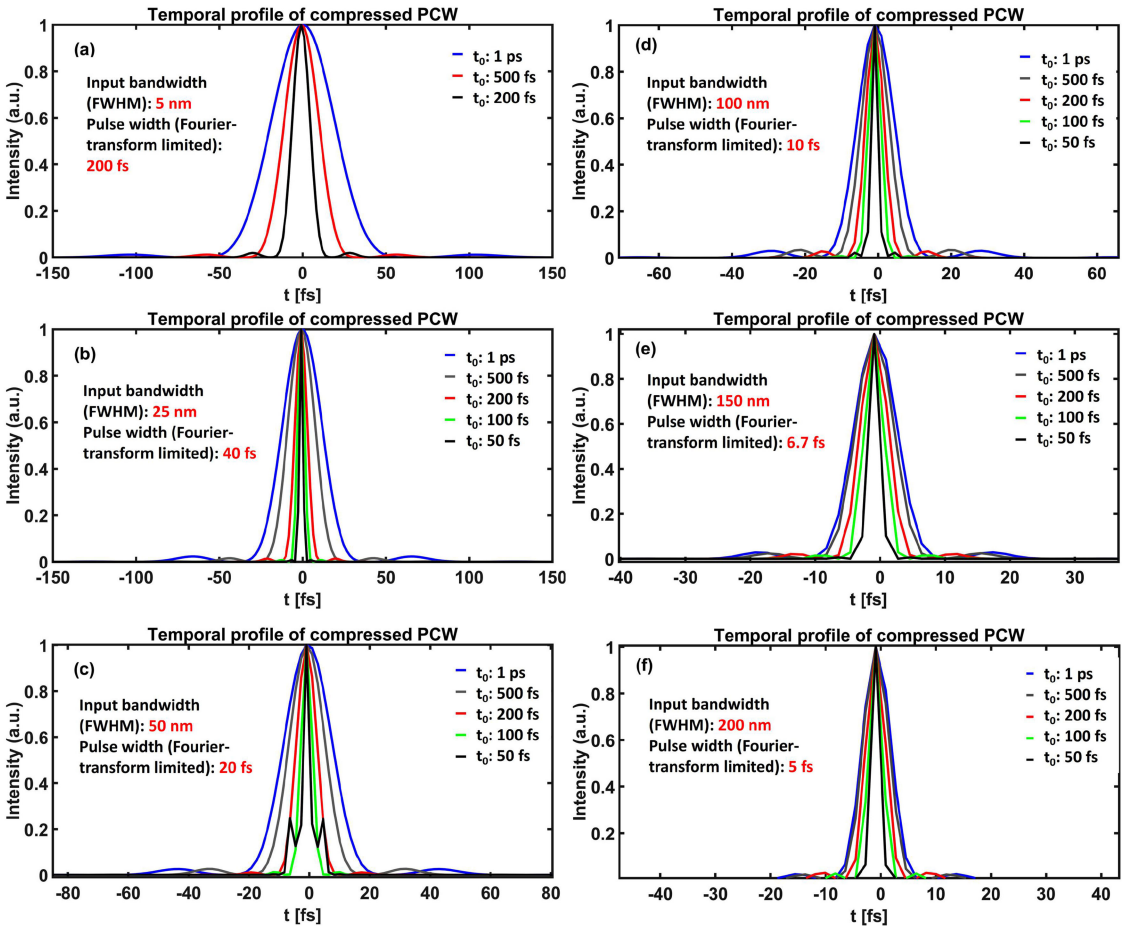

Fig. 7. Effects of initial chirp ratio and bandwidth on temporal profiles of the PCW after compression: (a) input fields with bandwidth of 5 nm and pulse widths of 1 ps, 500 fs, and 250 fs and (b)–(f) input bandwidth varied from 25 nm to 200 nm, with input pulse widths of 1 ps, 500 fs, 200 fs, 100 fs, and 50 fs.

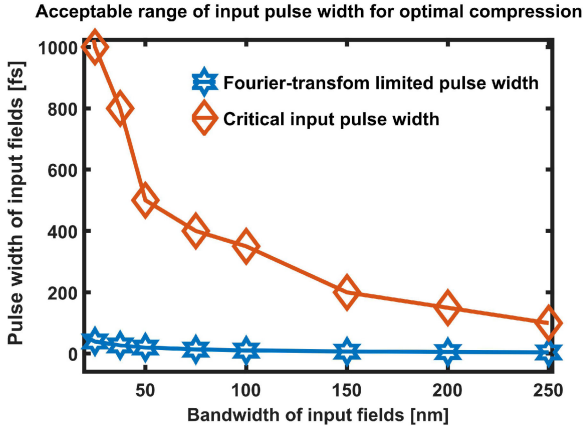

Fig. 8. Region of input pulse width for laser systems with different bandwidth, where the output PCW can be compressed to a minimal pulse width as narrow as that of the input fields. The red line indicates the “critical” input pulse widths that maintain the minimal compressible pulse width of the PCW and the blue line indicates the Fourier-transform limited pulse width of input fields.

pulse width is reduced from 1 ps to 50 fs. The simulation results also indicate that the pulse width of the PCW can be compressed to be even narrower than the Fourier-transform limit of the input fields owing to the broadened gain bandwidth during the DFWM process, which provides an opportunity to realize a higher output intensity.

Figure 8 shows a visualization of the suitable region of the input pulse width for laser systems with different bandwidths, where the minimal compressible pulse widths of the output PCW are not broader than those of input fields. The red line indicates the "critical" input pulse width that gives equal compressed pulse widths of the PCW compared with the input fields, while the blue line indicates the Fourier-transform limited pulse width of the input fields with different initial bandwidths. When the pulse width of input fields located within the region defined by the red line and blue line as shown in Fig. 8, a narrower pulse width of the PCW after compression compared with that of input fields can be realized. Figure 8 illustrates the systematic requirement for the input pulse width to maintain a minimal compressible pulse width for the DFWM process when utilized in laser systems with various bandwidths. As shown in Fig. 8, the operating region of the input pulse width significantly narrows as the initial bandwidth grows broader. For laser systems with an input bandwidth of 50 nm, the input pulse width for the DFWM process can be in the range of 50–500 fs, while for systems with an initial bandwidth of 250 nm, the critical pulse width drops to 100 fs. Another issue of concern is the duration of the pedestal noise of the compressed PCW. As discussed in Section 3.1.2, the pedestal noise of the PCW is mainly related to the pulse width of the input fields. The shorter the input pulse width, the narrower the pedestal region becomes. As a result, a careful adjustment of the input pulse width in the DFWM process greatly contributes to the optimization of the contrast enhancement performance and the minimum compressible pulse width.

3.3. Energy Conversion Efficiency

The energy conversion efficiency is another important parameter to evaluate the performance of a pulse cleaner in ultrashort laser systems, especially at extremely high energy. Simulation results indicated that the energy conversion efficiency is mainly affected by the GVD of a nonlinear medium, the initial pump–signal amplitude ratio κ, the spatial–temporal profiles of input fields and phase mismatching of input fields.

3.3.1 Effects of GVD: Positive GVD of a nonlinear medium introduces a linear up-chirp to the fields in the DFWM process, and vice versa. For initially positive chirped pulses incident on a medium with positive dispersion, the pulse width is broaden compared with incident fields if the nonlinear effects are relatively insignificant. Additionally, a positive GVD together with SPM and XPM results in a spectrum broadening at a higher speed without considering the PA effect. However, when considering the PA effect, a large value of GVD results in a decline in the maximum intensity as it broaden the pulse width, which unfavorably restricts the parametric process, and as a result, reduces the energy conversion efficiency of the PCW.

If the nonlinear medium has a negative GVD, both the signal and the PCW become narrower in the temporal profiles. Additionally, the pulse narrowing induced by GVD has a positive effect on the parametric process, resulting in a shorter interaction length. As shown in Table 1, a large value of GVD results in the reduction of the energy conversion efficiency regardless of its sign. Furthermore, a significant narrowing of the gain bandwidth occurs if GVD is sufficiently large ($>10^{-23}$ s^2/m). The effects of the higher order dispersion provide a nonlinear chirp on the fields in the DFWM process. According to the results in Table 1, a relatively strong intensity of input fields and mediums with large nonlinear susceptibility needs to be chosen to compromise the gain narrowing result from strong GVD via reducing the interaction length in the DFWM process. The effects of the higher order dispersion were neglected in this study due to their relatively low magnitude compared with GVD.

3.3.2 Effects of Pump–Signal Ratio: The initial pump–signal intensity ratio is also important in deciding the gain bandwidth and the conversion efficiency of the PCW. To evaluate its effects, GVD and the bandwidth of input fields are kept constant (In this case: $GVD = 3.62 \times 10^{-24}$ s^2/m and input bandwidth is 50 nm). The gain bandwidth and the energy conversion efficiency of the PCW

TABLE 1
Effects of GVD on the bandwidth and energy conversion efficiency of the PCW

GVD (s^2/m)	FWHM Bandwidth of input fields (nm)	10% Maximum Bandwidth of input fields (nm)	FWHM Bandwidth of PCW (nm)	10% Maximum Bandwidth of PCW (nm)	Energy conversion efficiency (%)	Optimal interaction length (mm)
-3.62×10^{-23}	50	91.3	**58.7**	**66.9**	**28.08**	**0.114**
-1.09×10^{-23}			64.3	76	36.47	0.204
-3.62×10^{-24}			68.8	79.3	39.17	0.264
-3.62×10^{-25}			75.8	85.4	41.35	0.327
-3.62×10^{-26}			75.5	85	41.80	0.345
0			75.5	87	41.86	0.345
3.62×10^{-26}			75.5	85.1	41.92	0.345
3.62×10^{-25}			75	84.5	42.21	0.345
3.62×10^{-24}			71.3	81.1	40.47	0.346
1.09×10^{-23}			65	75.2	39.41	0.36
3.62×10^{-23}			**58.8**	**69.8**	**38.87**	**0.618**

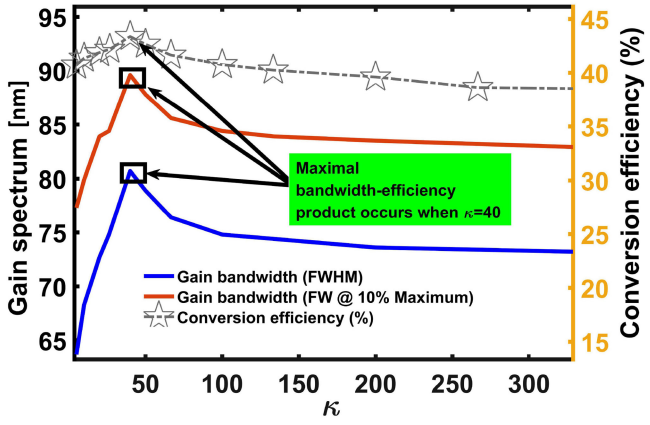

Fig. 9. Bandwidth and energy conversion efficiency of the PCW for different pump–signal amplitude ratios.

were numerically calculated, as shown in Fig. 9, the gain bandwidth of the PCW increases together with κ, reaching its maximum at $\kappa = 40$. Similarly, the energy conversion efficiency reaches its maximum at the same ratio. Fig. 9 verifies that the bandwidth efficiency product can be optimized by finding a balance between dispersion and the initial pump–signal intensity ratio for a laser system with a given bandwidth.

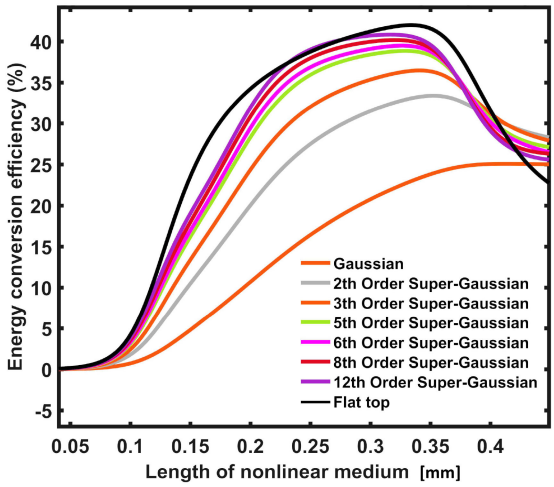

Fig. 10. Energy conversion efficiency of the PCW with different initial spatial profiles.

3.3.3 Spatial Effects: Spatial effects, such as spatial intensity distribution and spatial chirp, can also affect the conversion efficiency. To study these effects, we calculated the conversion efficiency with different spatial distributions. The simulation results are shown in Fig. 10. It can be seen that a conversion efficiency of 25% is achieved for input fields with a Gaussian spatial profile. The conversion efficiency increases as the spatial profile gradually becomes more uniform. The maximum value of the conversion is 42% for input fields with an uniform profile. It should be noted that a non-uniform spatial profile can also result in the deterioration of beam quality, such as small-scale self-focusing, filamentation, or even result in the damage of the nonlinear medium. Consequently, spatially uniform beams are preferred in the DFWM process.

If the input fields are spatially chirped (possibly generated by misalignment of stretchers or angular dispersion from optical elements in laser systems), even spatially uniformed input fields can affect the output PCW. The position-dependence of the spectrum can result in a phase-mismatch in the DFWM process, resulting in a reduction in conversion efficiency and a deterioration of beam quality. Moreover, linear and nonlinear spatial-chirps introduce a spatial-dependence in temporal and spectral profiles, and as a result, it strongly affects the compressed beam profile of the PCW. Thus, to realize a PCW with a large conversion efficiency and a high beam quality, the spatial chirp needs to be carefully eliminated or compensated for.

3.3.4 Effects of Phase Mismatching: As discussed in section 2, the phase matching condition of the DFWM process in an isotropic nonlinear medium is satisfied automatically when the input fields are perfectly coupled in temporal and spatial domains regardless of the wavelength and bandwidth of input fields. However, phase mismatching occurs in the DFWM process when angle-detuning of the two pumps existed. To optimize the DFWM process, the effects of phase mismatching should be detailed studied. A schematic image of the phase mismatching due to angle-detuning of pumps is shown in Fig. 11(a). The phase mismatch Δk can be calculated by Eq. (8):

$$\begin{aligned}\Delta k &= \left|\vec{k}_{Pump1} + \vec{k}_{Pump2} - \vec{k}_{Signal} - \vec{k}_{PCW}\right| \\ &= k_0(\lambda)\left\{\sqrt{1 + 4\sin\frac{1}{2}\theta \cdot \left[\sin\frac{1}{2}\theta - \sin\left(\varphi + \frac{1}{2}\theta\right)\right]} - 1\right\}. \end{aligned} \tag{8}$$

Where θ represents the detuning angle and ϕ describes the angle between one pump and the signal. Eq. (8) indicates that the phase mismatch Δk is governed by the detuning angle θ. The relationship between the phase mismatch Δk and angle-detuning is illustrated in Fig. 11(b).

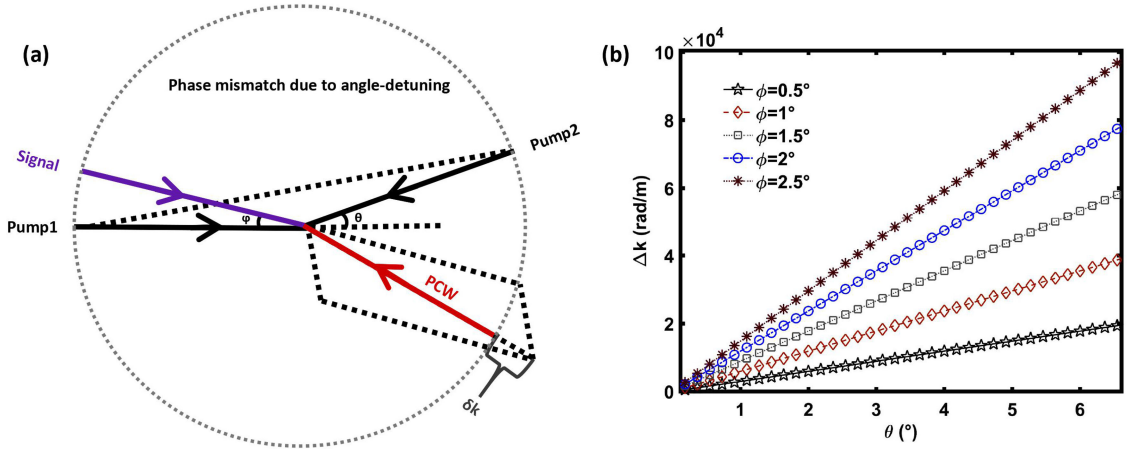

Fig. 11. Phase mismatching in the DFWM process due to angle-detuning: (a) a schematic image of phase mismatching due to angle-detuning; (b) relationship between the phase mismatch Δk and the detuning angle.

TABLE 2

Effects of phase mismatch on the bandwidth and energy conversion efficiency of the PCW

Δk (rad/m)	Input wavelength (nm)	FWHM Bandwidth of input fields (nm)	FWHM Bandwidth of PCW (nm)	Optimal interaction length (mm)	Energy conversion efficiency (%)
5×10^4	808	50	36.7	0.135	**14.49**
2.5×10^4			41.2	0.147	**22.19**
1×10^4			46.2	0.171	**27.98**
5×10^3			49.7	0.188	**30.82**
2.5×10^3			53.4	0.205	**33.04**
1000			59.6	0.23	**35.38**
500			62.5	0.246	**36.83**
250			65.3	0.264	**38.05**
100			68.1	0.286	**39.34**
50			69.7	0.3	**40.11**
0			73.8	0.34	**41.8**

As shown in Fig. 11(b), the phase mismatch Δk increases dramatically with the detuning angle, reaching 10^5 rad/m when $\theta = 6.5^\circ$ (in this case: $\phi = 2.5^\circ$).

The effects of phase mismatch was numerical investigated. As shown in Table 2, both the energy conversion efficiency and the gain bandwidth of the PCW reduced tremendously when the phase mismatch increased: the energy conversion efficiency reduced significantly from 42% to about 14.5% when $\Delta k = 5 \times 10^5$ rad/m while the gain bandwidth of the PCW became

TABLE 3
Summary of physical effects and their influences on the PCW

Physical effects and input parameters	Effects on the PCW
Initial chirp and bandwidth	Positive chirped pulse is suitable for the DFWM as it results in a broader bandwidth; negative chirped pulse is not suitable for the DFWM because the PCW has a significantly narrower bandwidth as the SPM- and XPM-induced frequency-chirp has a negative sign compared with the initial chirp.
SPM and XPM	Introducing frequency chirp to each field which strongly depends on the temporal profile and initial chirp of input fields: SPM and XPM result in spectrum broadening for positive-chirped inputs and narrowing for negative-chirped inputs.
Parametric amplification	The PCW is generated and amplified with a temporal and spectrum beam profile sharper than those of input fields; the contrast ratio of PCW is roughly cubic that of input fields before pulse compression; a pedestal noise with a region of a few ps is generated in the PA process and can be found when the PCW is compressed to femtosecond range. The length of the pedestal noise can be restricted by carefully choosing the input pulse width (initial chirp).
GVD	GVD of a nonlinear medium adopting a linear chirp to the fields evolving in the DFWM process: the larger the GVD, the lower the energy conversion efficiency and the narrower the gain bandwidth of the PCW; a positive GVD results in pulse broadening and an increase in the interaction length, while a negative GVD results in pulse narrowing and a reduction in the interaction length; large value of GVD results in narrowing of gain bandwidth and a reduction in energy conversion efficiency.
κ	The energy conversion efficiency and gain bandwidth varies when the ratio changes, the largest efficiency bandwidth product can be figured out.
Spatial intensity distribution	Maximal conversion efficiency achieved when the input fields have uniform spatial-distribution. The energy conversion efficiency of the PCW for inputs with Gaussian spatial profile reduces to 26%.
Phase mismatching	Phase mismatching results in a reduction in the energy conversion efficiency and narrowing in the gain bandwidth; the phase mismatching should be eliminated by a careful alignment of the input fields.
Spatial chirp	Input fields with a spatial chirp can result in a phase mismatch in the DFWM process, which results in the reduction of the conversion efficiency and degradation of the beam quality. This introduces a spatial-dependence in the temporal–spectral profiles and affects beam profile of the compressed PCW. Thus, the spatial chirp needs to be eliminated carefully.

narrower than that of input fields when $\Delta k = 5 \times 10^3$ rad/m. Eq. (8) also indicates that phase mismatch is affected by the wavelength and bandwidth of input fields. A broad bandwidth of input fields results in distortion in temporal profile and reduction of conversion efficiency when the detuning angle is given: the higher the input frequency, the larger the phase mismatch became and consequently, the lower the conversion efficiency. As a result, in order to maintain a large

TABLE 4
Selective nonlinear mediums for high-efficiency PCW generation

Glass composition		Refractive Index	Susceptibility (ESU)	Transmission bandwidth (μm)	Nonlinear response time (fs)	Ref.
Chalcogenide glasses	NOG–4 (Ge–As–S–Se)	2.55 (0.633)	7.0×10^{-12}	0.7–16	< 400	[37]
	As_2S_3	2.53 (0.633)	7.2×10^{-12}			
Tellurite glass	TeO_2	2.239 (0.633)	1.4×10^{-12}	0.35–6	< 200	[38]
	$25PbO–10TiO_2–65TeO_2$	2.27 (0.633)	3.7×10^{-12}			
	$10Nb_2O_8–10TiO_2–80TeO_2$	2.18 (0.633)	1.2×10^{-12}			
Bismuth acid glass	$42.5Bi_2O_3–28.4Si_2O_3–28.4B_2O_3–0.7CeO_2$	2.05	9.3×10^{-12}	0.45–5	< 200	[38] [39][40]
	MOx–Li2O–ZnO–Bi_2O_3	2.1–2.31	6×10^{-12} -49×10^{-12}			
	$Bi_2O_3–B_2O_3–SiO_2$	1.87–2.21	5.3×10^{-12} -9.3×10^{-12}			

efficiency bandwidth product, the detuning angle should be carefully eliminated (i.e., $\phi \leq 1^\circ$ and $\theta \leq 0.1^\circ$).

4. Discussions

A specific discussion of physical effects on the PCW are summarized in Table 3.

As shown in Table 3, the SPM and XPM combined with an initially positive-chirp can potentially result in a spectrum broadening of the PCW, while the PA can result in narrowing in both the temporal pulse width and gain bandwidth of spectrum. The PA also result in a pedestal noise when the PCW is compressed. The temporal interval of this pedestal noise is fundamentally decided by pulse width and bandwidth of initial fields in the DFWM process. The gain bandwidth of the PCW can be optimized by wisely choosing the pulse width of input fields to realize a minimal compressible pulse width. The energy conversion efficiency of the PCW is mainly affected by the GVD, the temporal–spatial profile, the phase mismatch and the ratio of the initial pump–signal intensity. Thus, to achieve a large efficiency bandwidth product while maintaining a desirable contrast enhancement capability, the initial chirp needs to be positive, and a suitable intensity (several GW/cm^2), a relatively narrow pulse width of input fields, suitable intensity ratio of input fields, and low thickness of the nonlinear medium are preferred. Also, the phase-matching condition and temporal-spatial coupling of input fields should be precisely maintained.

Another important issue of concern is the choice of an ideal nonlinear medium. As mentioned previously, an optimal nonlinear medium for the DFWM process needs to be centrally symmetric and isotropic to ensure that second-order nonlinear effects do not arise and the phase-matching condition can be satisfied easily. Moreover, the medium also needs to have a large third-order susceptibility, a short nonlinear response time, and a broad transmission bandwidth. A number of potential mediums for PCW generation are listed in Table 4.

5. Conclusions

In this paper, we presented an in-depth research on the PCW generation in the DFWM process and on its potential as a pulse cleaner in petawatt ultrashort laser systems. The numerical simulations were carried out focusing on the contrast enhancement capability, gain bandwidth, and energy conversion efficiency for systematic evaluation of the performance as pulse cleaners. Specifically, a recursive formula was proposed to numerically determine the contrast ratio of the PCW directly after the DFWM process. The contrast ratio of the PCW is roughly cubic that of the input fields. When the PCW is compressed, a pedestal noise within a region of a few ps was found. The origin and the removal method of this pedestal were studied. Next, we examined the optimization method of the gain bandwidth of the PCW to realize a minimal compressible pulse width. A systematical requirement for the input pulse width in the DFWM process was provided for laser systems with different bandwidths. Additionally, the simulation results proves that the conversion efficiency is mainly influenced by spatial–temporal profile, the phase mismatch and pump–signal intensity ratio of input fields. It was also verified that a considerably large efficiency bandwidth product and an excellent contrast enhancement capacity can be realized by finding the balance between each physical effect and input parameters. In summary, the potential of PCW generation via the DFWM process as a pulse cleaner in femtosecond high-power laser systems were studied comprehensively. Guidance have been proposed in the numerical analysis for laser systems with a wide range of bandwidth.

References

[1] D. Strickland and G. Mourou, "Compression of amplified chirped optical pulses," *Opt. Commun.*, vol. 55, no. 6, pp. 447–449, 1985.

[2] N. Hopps *et al.*, "Overview of laser systems for the Orion facility at the AWE," *Appl. Opt.*, vol. 52, no. 15, pp. 3597–3607, 2013.

[3] S. W. Bahk *et al.*, "Generation and characterization of the highest laser intensities (1022 W/cm^2)," *Opt. Lett.*, vol. 29, no. 24, pp. 2837–2839, 2004.

[4] J. D. Zuegel *et al.*, "Laser challenges for fast ignition," *J. Fusion Sci. Technol.*, vol. 49, no. 3, pp. 453–482, 2006.

[5] M. Hornung *et al.*, "The all-diode-pumped laser system POLARIS—An experimentalist's tool generating ultra-high contrast pulses with high energy," *High Power Laser Sci. Eng.*, vol. 2, no. 3, pp. 5–11, 2014.

[6] M. Nantel *et al.*, "Temporal contrast in Ti:sapphire lasers, characterization and control," *IEEE J. Sel. Topics Quantum Electron.*, vol. 4, no. 2, pp. 449–458, Mar./Apr. 1998.

[7] B. Dromey *et al.*, "High harmonic generation in the relativistic limit," *Nature Phys.*, vol. 2, no. 7, pp. 449–462, 2006.

[8] H. Kiriyama *et al.*, "High-energy, high-contrast, multiterawatt laser pulses by optical parametric chirped-pulse amplification," *Opt. Lett.*, vol. 32, no. 16, pp. 2315–2317, 2007.

[9] G. A. Mourou, C. L. Labaune, M. Dunne, N. Naumova, and V. T. Tikhonchuk, "Relativistic laser-matter interaction: From attosecond pulse generation to fast ignition," *Plasma Phys. Controlled Fusion*, vol. 49, no. 12B, pp. B667–B675, 2007.

[10] P. Antici *et al.*, "Energetic protons generated by ultrahigh contrast laser pulses interacting with ultrathin targets," *Phys. Plasmas*, vol. 14, no. 3, 2007, Art. no. 030701.

[11] G. Kulcsár *et al.*, "Intense picosecond X-ray pulses from laser plasmas by use of nanostructured "Velvet" targets," *Phys. Rev. Lett.*, vol. 84, no. 22, pp. 5149–5152, 2000.

[12] J. Itatani, J. Faure, M. Nantel, G. Mourou, and S. Watanabe, "Suppression of the amplified spontaneous emission in chirped-pulse-amplification lasers by clean high-energy seed-pulse injection," *Opt. Commun.*, vol. 148 no. 1–3, pp. 70–74, 1998.

[13] A. Renault *et al.*, "ASE contrast improvement with a non-linear filtering Sagnac interferometer," *Opt. Commun.*, vol. 248, no. 4–6, pp. 535–541, 2005.

[14] M. P. Kalashnikov, E. Risse, H. Schönnagel, and W. Sandner, "Double chirped-pulse-amplification laser: A way to clean pulses temporally," *Opt. Lett.*, vol. 30, no. 8, pp. 923–925, 2005.

[15] A. Jullien *et al.*, "High-efficiency, simple setup for pulse cleaning at the millijoule level by nonlinear induced birefringence," *Opt. Lett.*, vol. 29 no. 18, pp. 2184–2186, 2004.

[16] G. I. Petrov, O. Albert, J. Etchepare, and S. M. Saltiel, "Cross-polarized wave generation by effective cubic nonlinear optical interaction," *Opt. Lett.*, vol. 26, no. 6, pp. 355–357, 2001.
[17] R. C. Shah, R. P. Johnson, T. Shimada, K. A. Flippo, J. C. Fernandez, and B. M. Hegelich, "High-temporal contrast using low-gain optical parametric amplification," *Opt. Lett.*, vol. 34, no. 15, pp. 2273–2275, 2009.
[18] J. Liu, K. Okamura, Y. Kida, and T. Kobayashi, "Temporal contrast enhancement of femtosecond pulses by a self-diffraction process in a bulk Kerr medium," *Opt. Exp.*, vol. 18, no. 21, pp. 22245–22254, 2010.
[19] D. Hillier *et al.*, "Ultrahigh contrast from a frequency-doubled chirped-pulse-amplification beamline," *Appl. Opt.*, vol. 52, no. 18, pp. 4258–4263, 2013.
[20] J. Wang, J. Ma, Y. Wang, P. Yuan, G. Xie, and L. Qian, "Noise filtering in parametric amplification by dressing the seed beam with spatial chirp," *Opt. Lett.*, vol. 39, no. 8, pp. 2439–2442, 2014.
[21] B. Gilicze, R. Dajka, I. B. Földes, and S. Szatmári, "Improvement of the temporal and spatial contrast of the nonlinear Fourier-filter," *Opt. Exp.*, vol. 25, no. 17, pp. 20791–20797, 2017.
[22] Z. Ma and S. Li, "Theoretical analysis of ASE contrast improvement with a rapid scanning F-P interferometer in a CPA system," *J. Opt.*, vol. 14, no. 7, pp. 565–570, 2012.
[23] H. C. Kapteyn, M. M. Murnane, A. Szoke, and R. W. Falcone, "Prepulse energy suppression for high-energy ultrashort pulses using self-induced plasma shuttering," *Opt. Lett.*, vol. 16, no. 7, pp. 490–492, 1991.
[24] I. Musgrave *et al.*, "Picosecond optical parametric chirped pulse amplifier as a preamplifier to generate high-energy seed pulses for contrast enhancement," *Appl. Opt.*, vol. 49, no. 33, pp. 6558–6562, 2010.
[25] C. Dorrer, A. Consentino, D. Irwin, J. Qiao, and J. D. Zuegel, "OPCPA front end and contrast optimization for the OMEGA EP kilojoule, picosecond laser," *J. Opt.*, vol. 17, no. 9, 2015, Art. no. 094007.
[26] Y. Arikawa *et al.*, "Ultrahigh-contrast kilojoule-class petawatt LFEX laser using a plasma mirror," *Appl. Opt.*, vol. 55, no. 25, pp. 6850–6857, 2016.
[27] D. Hillier *et al.*, "Ultrahigh contrast from a frequency-doubled chirped-pulse-amplification beamline," *Appl. Opt.*, vol. 52, no. 18, pp. 4258–4263, 2013.
[28] J. Zhu *et al.*, "Analysis and construction status of SG-II 5PW laser facility," *High Power Laser Sci. Eng.*, vol. 6, no. 2, pp. 115–127, 2018.
[29] F. Wei *et al.*, "Progress of the injection laser system of SG-II," *High Power Laser Sci. Eng.*, vol. 6, 2018, Art. no. e34.
[30] J. Zhaoyang *et al.*, "Design and performance of final optics assembly in SG-II Upgrade laser facility," *High Power Laser Sci. Eng.*, vol. 6, 2018, Art. no. e14.
[31] S. G. Liang, H. J. Liu, N. Huang, Q. B. Sun, Y. S. Wang, and W. Zhao, "Temporal contrast enhancement of picosecond pulses based on phase-conjugate wave generation," *Opt. Lett.*, vol. 37, no. 2, pp. 41–43, 2012.
[32] A. Yariv and D. M. Pepper, "Amplified reflection, phase conjugation, and oscillation in degenerate four-wave mixing," *Opt. Lett.*, vol. 1, no. 1, pp. 16–18, 1977.
[33] S. A. Lesnik *et al.*, "Laser with a stimulated-Brillouin-scattering complex-conjugate mirror," *Zhurnal Tekhnicheskoi Fiziki*, vol. 49, pp. 2257–2259, 1979.
[34] G. S. He, Y. Cui, M. Yoshida, and P. N. Prasad, "Phase-conjugate backward stimulated emission from a two-photon-pumped lasing medium," *Opt. Lett.*, vol. 22, no. 1, pp. 10–12, 1997.
[35] H.-F. Yau, P.-J. Wang, E.-Y. Pan, and J. Chen, "Self-pumped phase conjugation with femtosecond pulses by use of $BaTiO_3$," *Opt. Lett.*, vol. 21, no. 15, pp. 1168–1170, 1996.
[36] M. B. Danailov, K. Diomande, P. Apai, and R. Szipocs, "Phase conjugation of broad-band laser pulses in $BaTiO_3$," *Optica Acta: Int. J. Opt.*, vol. 45, no. 1, pp. 5–9, 1998.
[37] H. Nasu, J. Matsuoka, and K. Kamiya, "Second- and third-order optical non-linearity of homogeneous glasses," *Japanese J. Appl. Phys. Suppl.*, vol. 37, no. 19, pp. 23–30, 1994.
[38] N. Sugimoto, H. Kanbara, S. Fujiwara, K. Tanaka, Y. Shimizugawa, and K. Hirao, "Third-order optical nonlinearities and their ultrafast response in Bi_2O_3-B_2O_3-SiO_2 glasses," *J. Opt. Soc. Amer. B*, vol. 16, pp. 1904–1908, 1999.
[39] N. Sugimoto, H. Kanbara, S. Fujiwara, K. Tanaka, and K. Hirao, "Ultrafast response of third-order optical nonlinearity in glasses containing Bi_2O_3," *Opt. Lett.*, vol. 21, pp. 1637–1639, 1996.
[40] T. Hasegawa, T. Nagashima, and N. Sugimoto, "Z-scan study of third-order optical nonlinearities in bismuth-based glasses," *Opt. Commun.*, vol. 250, pp. 411–415, 2005.